LAWRENCE
LIVERMORE
NATIONAL
LABORATORY

LLNL-JRNL-423070

Plastic ablator ignition capsule design for the National Ignition Facility

D. S. Clark, S. W. Haan, B. A. Hammel, J. D. Salmonson, D. A. Callahan, R. P. Town

February 2, 2010

Physics of Plasmas

Disclaimer

Plastic ablator ignition capsule design for the National Ignition Facility

Daniel S. Clark,* Steven W. Haan, Bruce A. Hammel, Jay D. Salmonson, Debra A. Callahan, and Richard P. J. Town
Lawrence Livermore National Laboratory, Livermore, California 94550
(Dated: January 19, 2010)

The National Ignition Campaign, tasked with designing and fielding targets for fusion ignition experiments on the National Ignition Facility (NIF), has carried forward three complementary target designs for the past several years: a beryllium ablator design, a plastic ablator design, and a high-density carbon or synthetic diamond design. This paper describes current simulations and design optimization to develop the plastic ablator capsule design as a candidate for the first ignition attempt on NIF. The trade-offs in capsule scale and laser energy that must be made to achieve a comparable ignition probability to that with beryllium are emphasized. Large numbers of 1-D simulations, meant to assess the statistical behavior of the target design, as well as 2-D simulations to assess the target's susceptibility to Rayleigh-Taylor growth are presented.

PACS numbers:

I. INTRODUCTION

The National Ignition Facility (NIF) is a 1.8 MJ laser facility designed to achieve Inertial Confinement Fusion (ICF) ignition as part of the National Ignition Campaign (NIC) [1, 2]. Full scale ignition targets are planned to use $1.2 - 1.8$ MJ of frequency tripled (near ultra violet) light directed into a uranium hohlraum to implode and ignite a capsule containing deuterium-tritium (DT) fuel. Successful fusion ignition on NIF will represent the culmination of several decades' research into laser design and construction, laser-plasma interactions, hohlraum physics, and finally capsule implosion physics and optimization [3]. For the last of these research areas, extensive work has focused on maximizing the robustness of the capsule design to both uncertainties in the physics of the implosion (principally, material opacities and equations of state, laser absorption and x-ray generation and transport, and hydrodynamic instability growth) and inevitable defects and uncertainties in the fabrication of the capsule. Detailed capsule designs hence represent highly optimized designs not only in the sense of optimizing for the models believed to be the closest representation of reality but also in the sense of accommodating uncertainties in those models.

The very early phases of capsule design for NIF focused on plastic ablator targets uniformly doped with bromine, the high-Z bromine being introduced to attenuate the x-ray flux through the ablator which would otherwise preheat the DT fuel to an unacceptable degree [4]. In an effort to improve capsule performance, beryllium doped with copper was proposed as an ablator and shown, in simulations, to be markedly more stable hydrodynamically than plastic [5, 6]. Nearly concurrently, graded doped designs were introduced for both copper-doped beryllium [7] and later germanium-doped plastic. In these designs, the high-Z dopant is concentrated in a relatively thin layer near the fuel-ablator interface. Since the thin inner layer of undoped ablator next to the fuel is thereby substantially shielded from the x-ray flux and hence remains cold and dense, the density discontinuity between the DT fuel and ablator is reduced and the possibility of deleterious mix between the two lessened. Simultaneously, the penalty of a reduced ablation pressure and velocity due to the presence of dopant in the outer regions of the ablator is avoided. In simulations, these graded-dopant designs proved decisively superior to uniformly doped designs and have hence been adopted as the standard capsule configuration [8].

Currently, three types of ablator material are under study for the NIC ignition capsule: beryllium doped with copper; plastic, referred to as CH, doped with germanium; and nano-crystalline synthetic diamond, also known as high-density carbon, doped with tantalum. Each of these materials shows various strengths and weaknesses that recommend it as the first choice ablator. Equally, each of these capsule ablator materials has been intensively investigated both theoretically and experimental. This paper summarizes the current state of the CH capsule design, as represented by a large data base of simulations run with the radiation hydrodynamics code LASNEX [9]. As these designs constantly evolve in response to improved physics modeling and the input of experimental data, it should be recognized that this paper is necessarily a snapshot of a continuing work in progress.

This paper is organized as follows. Sec. II begins by summarizing the relative strengths and weaknesses of beryllium and CH as ablator materials. This comparison conveniently serves to illustrate the many trade-offs to be made in capsule design, not merely between laser performance and capsule stability, but also within the limits of what is actually fabricable. Sec. III then presents the one-dimensional (1-D) considerations that are the foundation of the capsule design. Sec. IV summarizes the two-dimensional (2-D) low-mode simulations that are used to assess the robustness of the capsule design to perturbations to the igniting hot spot. As an example, two of

*Electronic address:clark90@llnl.gov

the deviations from the nominal design which can impact the ignition of the hot spot are investigated in this way. Sec. V then extends these 2-D simulations to investigations of growth at intermediate mode wavelengths. The sensitivity of these intermediate mode growth factors to the CH equation of state (EOS) and to the strength of the first shock used in driving the capsule are highlighted. The growth of isolated defects on the surface of the capsule which occur in this wavelength range are also discussed. Sec. VI then presents a statistical assessment of the capsule reliability to all expected manufacturing and physics uncertainties in both 1-D and 2-D. Finally, illustrative of the continuing evolution of the design, Sec. VII summarizes some resent design modifications as a result of continuing design optimization and in the light of recent sub-ignition NIF experiments. Sec. VIII concludes.

II. CHARACTERISTICS OF BERYLLIUM AND PLASTIC ABLATORS

As ablator materials, beryllium and CH exhibit complementary strengths and weaknesses. Foremost from the perspective of ICF capsule design is the relative susceptibility of each material to hydrodynamic instability growth during implosion. Principally, these are the Richtmyer-Meshkov (RM) and Rayleigh-Taylor (RT) instabilities active during the initial shock and later acceleration phases of the implosion, respectively. Unquestionably, beryllium, on account of its higher density and higher ablation velocity, is more stable hydrodynamically than CH [6]. It was this factor that initially motivated the investigation of beryllium as an ablator material.

RT and RM growth must develop from the seed level set by the initial capsule roughness or other imperfections, and in this respect, the disadvantageous lower ablation rate of CH is offset somewhat by the its smoother initial surface. While beryllium shells can be polished to a surfaces finish of $\sim 20\,\mathrm{nm}$ overall roughness, fabricated plastic shells have an inherent roughness of only $\sim 10\,\mathrm{nm}$. This greater smoothness of plastic does not fully offset its lower ablation rate, however, and at this level of detail beryllium ablators still result in net less perturbed implosions than their CH counterparts.

Average surface roughness alone does not fully characterize an ablator's seeds for hydrodynamic instability, however. Both beryllium and CH have subtle isolated defects and internal structure that have proven to be significant influences on both designs. In the case of beryllium, since the beryllium (and its copper dopant) are deposited in a sputtering process, fabricated shells have been found to display micro-structure in the form of volumes of lowered density relative to the average, referred to as "sponge blobs." Sputter-deposited beryllium also includes a variety of trace impurities, most notably argon. In addition to reducing the ablation velocity achievable with beryllium, this argon impurity has also been found to be inhomogeneously distributed in the shell. Both the "sponge blobs" and argon variability serve as an extended, volumetric seed for RT growth. Quite recently, it has also been observed that the copper dopant added to beryllium migrates non-uniformly as the shells are heated to remove the initial interior mandrel. The opacity and density perturbation introduced by this migration is yet another substantial seed for RT growth.

By contrast, other than the presence of oxygen, CH has no known impurities or internal micro-structure. The graded germanium dopant is chemically bonded into the CH polymer and is not believed to migrate. A compensating defect of CH, however, is the presence of isolated surface imperfections on the inner and outer surfaces of CH shells. These imperfections amount to typically many dozens of bumps approximately 100 nm in height and $10\,\mu\mathrm{m}$ in width. As discussed in Sec. V below, these bumps can lead to jets of ablator material penetrating into the hot spot at ignition time.

Coupled to the general hydrodynamic stability of these ablators is also the presence of the glass fill tubes used to inject the DT fuel (as a liquid) into ignition capsules. As these fill tubes will remain in place during the implosion, they represent quite substantial seeds for instability growth [10]. Simulations suggest that the presence of the fill tube on CH capsules results in the injection of $\sim 30\,\mathrm{ng}$ of ablator material as a jet into the hot spot. By contrast, for the more stable beryllium ablators, a comparable fill tube injects only $\sim 15\,\mathrm{ng}$ of material. The quantitative impact of this larger mass of contaminants is discussed in Sec. IV.

On account of its generally larger amount of instability growth and larger mass of contaminants in the hot spot (introduced by the fill tube), a CH capsule must be larger in scale and driven with more laser energy at a higher power and radiation temperature to be comparably robust to a beryllium ablator counterpart. The current beryllium capsule design, for example, calls for 1.3 MJ of energy and 380 TW whereas the CH design requires 1.55 MJ of energy and 450 TW, including allowances for backscatter. CH capsules then effectively put more stress on the laser system to deliver the required power and energy. On the other hand, though the laser power and energy are higher in the CH design, the presence of a multi-species plasma resulting from the blow-off from a CH ablator should be less susceptible to stimulated Brillouin scatter than the single-species beryllium plasma. Current estimates suggest that with respect to the growth of laser-plasma scattering instabilities, beryllium plasmas driven at a radiation temperature of 285 eV are comparable to CH plasmas driven at 300 eV.

Finally, in addition to these differences in the ablation physics of beryllium and CH, there are two technological differences which distinguish these ablators. First, since CH is transparent to optical radiation, it has been proposed that the initial roughness of the inner DT ice surface, a significant contributor to the ultimate degree of hot spot asymmetry at ignition time, might be diagnosed optically before an ignition attempt. In this way, espe-

cially rough ice layers might be detected *in situ*, melted, and refrozen into a higher quality layer, and so the ignition probability per shot increased. Since beryllium is opaque to optical frequencies, a more complicated x-ray technique is required for this ablator which yields less information about the layer's quality. While there are currently no plans to exploit this pre-shot layer characterization with CH, it remains a contingency possibility if ignition is not achieved as reliably as desired. Second, regulatory constraints on the use of beryllium significantly add to the complexity of operations. In the interest of efficiently gathering data from as large a number of shots as possible, this is an additional advantage of CH. And lastly, while beryllium must be recognized as a clearly superior ablator material from the perspective of RT growth, it should also be recognized that the understanding of the performance of CH ablators rest on a much more extensive experimental data base than for beryllium. In this respect, though CH's performance is inferior, it is importantly less uncertain.

Despite its inferior stability properties relative to beryllium, several modifications have recently increased the viability of the CH capsule design. Most significantly, relative to previous designs, the scale of the capsule and laser energy used to drive the hohlraum have been increased from an outer radius of 1092 μm to 1160 μm and from 1.25 MJ to 1.55 MJ, respectively. As already mentioned, the scale increase was driven from a requirement to match the robustness properties of the CH capsule to those of beryllium and was enabled by the projection that the NIF laser would reliability be able to deliver pulses in the range of 1.5 MJ. Secondly, to reduce the capsules susceptibility to hydrodynamic instability growth, the ablator was thickened from 165 μm to 190 μm, while the fuel thickness was reduced from 75 μm to 63 μm to maintain, as much as possible, the capsule implosion velocity. Thirdly, the radiation temperature at the "foot" of the pulse used to drive the first shock into the capsule has been reduced from 88 eV to 74 eV. This change significantly reduces the expected RT growth as described in Sec. V. Finally, the simulations used to assess the design's performance have been run with the latest tabular EOS for plastic. This EOS table has been calibrated against recent experiments and is believed to be a better representation of the behavior of compressing CH. As discussed below, the compressibility of the CH has been found strongly to impact the amount of instability growth.

III. ONE-DIMENSIONAL DESIGN CONSIDERATIONS

The CH ablator capsule designs discussed here are shown in Fig. 1. The designs are designated "Rev. 4" and "Rev. 4 draft 1." These names arise from the sequence of major revisions that the capsule has undergone in the context of the NIC program; Rev. 4 draft 1 represents a preliminary version of the final Rev. 4 design. Most of the results presented below apply to the draft 1 design with the developments leading to the final Rev. 4 design discussed in Sec. VII.

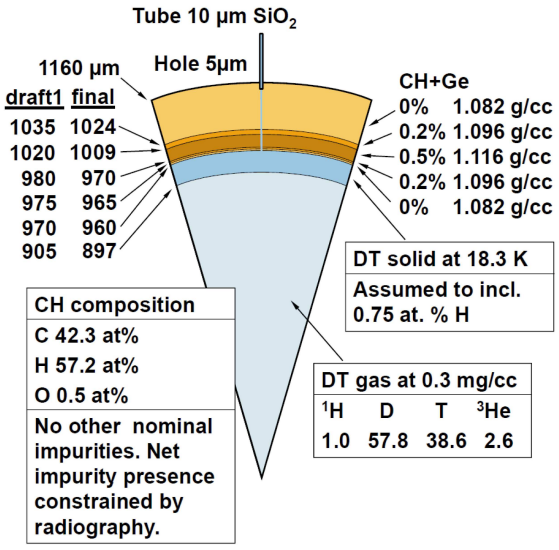

FIG. 1: (Color on-line) "Pie diagram" of the recent versions of the CH capsule design termed Rev. 4. The left column of dimensions corresponds to an early draft 1 version of the design and the right column to the final design. Most of the results described below pertain to the draft 1 version of the design with the evolution to the final design discussed in Sec. VII.

As with all of the ignition capsule designs, a layer of cryogenic DT ice lines the inside of a spherical ablator shell. The temperature at which the capsule is fielded (18.3 K in this case) determines the DT gas density of the central void (0.3 mg/cm^3). As already described, the inner region of the ablator is doped with a high-Z material (in this case germanium) to adjust the x-ray opacity, while the outer region which makes up the majority of the material ablated is left undoped. Typically, the dopant is arranged in three layers of successively increasing and then decreasing concentration to moderate the discontinuity introduced in the density distribution. Note that this introduction of a high-Z component to the ablator is advantageous for the stability of the fuel ablator interface, but, once the ablation wave has reached the dopant column, the presence of the dopant steepens the ablation front leading to higher RT growth there as well as a reduction in the ablation pressure and ultimate implosion velocity.

In addition to the capsule dimensions and compositions, the 1-D design is characterized by a tuned radiation pulse shape giving good entropy and implosion velocity. Fig. 2 shows the radiation temperature pulse shape used to drive the capsule. The radiation temperature is extracted from an integrated hohlraum simulation including laser beam propagation and absorption and accounting for expected losses due to laser-plasma interactions.

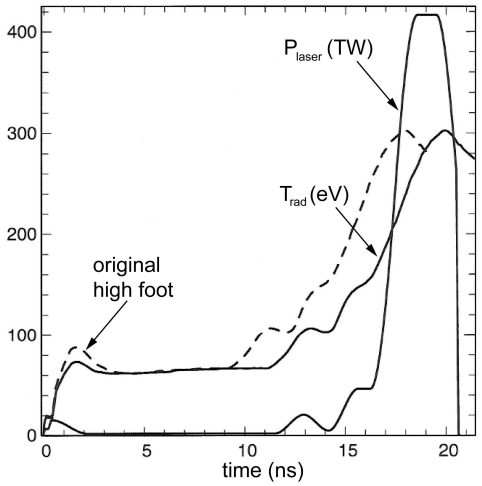

FIG. 2: Four-step 300 eV pulse shape used to drive the Rev. 4 CH capsule. The photon spectrum represented by this radiation temperature is extracted from an integrated hohlraum simulation driven with the total laser power also shown. The dashed curve shows an earlier high-foot pulse shape used for the capsule as discussed in Sec. V.

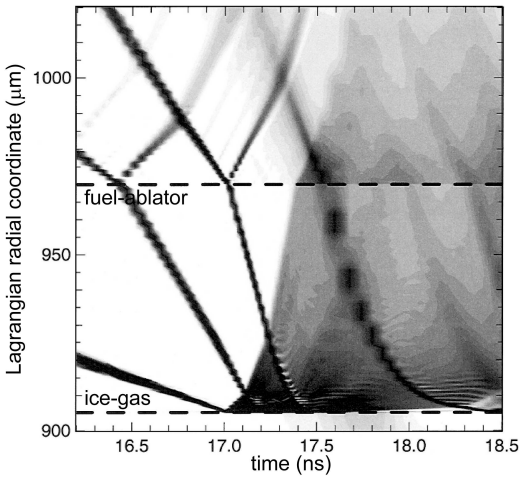

FIG. 3: Plot of the logarithmic radial derivative of the hydrodynamic pressure versus time and Lagrangian radius. The dashed lines denote the ice-gas interface and the fuel-ablator interface. The four shocks are seen transiting the DT fuel layer and breaking out into the DT gas. Following the first shock breakout, a rarefaction propagates outwards towards the fuel-ablator interface. Successive shocks crossing this rarefaction increase the fuel entropy requiring that the shocks breakout in the tight sequence shown.

The total laser power used for the integrated hohlraum simulation is also shown in the figure. Note that the radiation source used in the capsule implosion simulations includes the non-Planckian character of the radiation field which affects significantly the hydrodynamic stability.

The pulse shape shows the characteristic four-shock structure of steps in the radiation temperature at 2, 12, 14, and finally 17 ns. The levels of these steps and their temporal spacing are adjusted to tune the passage of the four shocks through the DT fuel. As illustrated in Fig. 3, once properly tuned these shocks break out in a close sequence $100-200$ ps apart at the inner edge of the DT ice. Too loose a spacing of the shock breakout will lead to too much entropy generation in the fuel and degrade its compressibility; too tight a spacing increases the likelihood of shock overtaking in the experiment also leading to excessive fuel entropy. In addition to the timing, the strength of the shocks are chosen so that the entropy increase with each shock's passage is an incremental contribution to the total, large disparities in shock strengths tending to generate overall higher fuel entropies. The deposited fuel entropy in this design is plotted in Fig. 4 against normalized fuel mass for a sequence of times. The four entropy plateaus corresponding to the passage of the four successive shocks show the successive steps in entropy up to its nearly constant in-flight value. As a measure of the implosion adiabat, we first calculate the mass-averaged fuel entropy at peak velocity. The pressure on this isentrope at $1,000\,\mathrm{g/cm^3}$ is then compared to the minimum pressure at that density (as given by the EOS table used in the simulation), and that ratio is interpreted as the fuel averaged adiabat. With this definition, the adiabat for the design is 1.51. The peak implosion velocity for the design, computed from the square root of the fuel averaged kinetic energy, is 0.384 mm/ns.

Once the 1-D considerations of implosion velocity and entropy have been adequately tuned, the 2-D and 3-D considerations of hydrodynamic stability can be addressed. Already in 1-D, however, the first contributor to hydrodynamic stability can be adjusted in the form of the 1-D shell density profiles during the implosion. As discussed above, these density profiles can be modified by adjusting the distribution and concentration of dopants in the shell. Fig. 5 illustrates how the width and peak concentration of the ablator's initial dopant column can be adjusted to modify the density distribution at peak velocity. To avoid reducing the implosion velocity, these four dopant distributions were all constrained to have a dopant column width proportional to the inverse square root of the peak dopant concentration [11]. By increasing the dopant concentration, the Atwood number which develops between the DT fuel and the unablated plastic can be reduced. For controlling the development of high-mode mix of ablator material into the fuel at this interface, reducing this Atwood number is an important stabilizing effect [12]. However, this reduced Atwood number can be seen to come at the cost of increasing the steepness of the ablation front at the outside of the shell. This effect is to be expected since it is the most heavily doped layer of the ablator that is typically being ablated at peak velocity which, with a higher concentration of dopant, will lead to a steeper ablation front. Clearly, this steepening is deleterious to the stability of the ablation front, and a trade-off must be made between stability of the fuel-ablator interface and the ablation front. More quan-

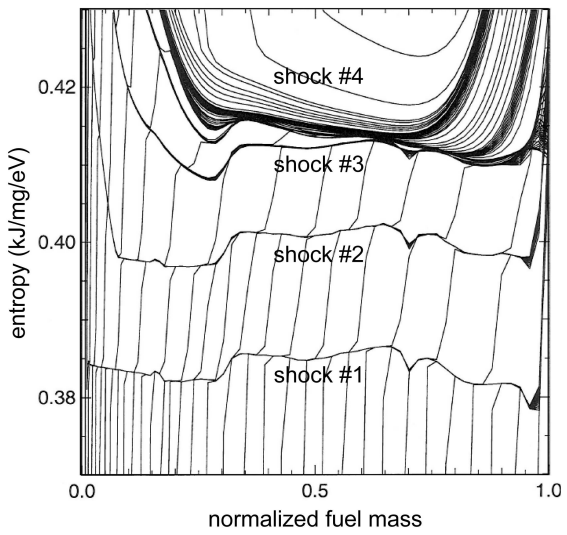

FIG. 4: Plot of the entropy deposited in the DT fuel versus normalized fuel mass for a succession of times. The four horizontal plateaus show the nearly uniform entropy deposited by each shock as it crosses the fuel. Entropy generated by heat conduction from the ablator into the outer fuel region and the high entropy deposited at the inside of the fuel by the passage of the fourth shock are evident.

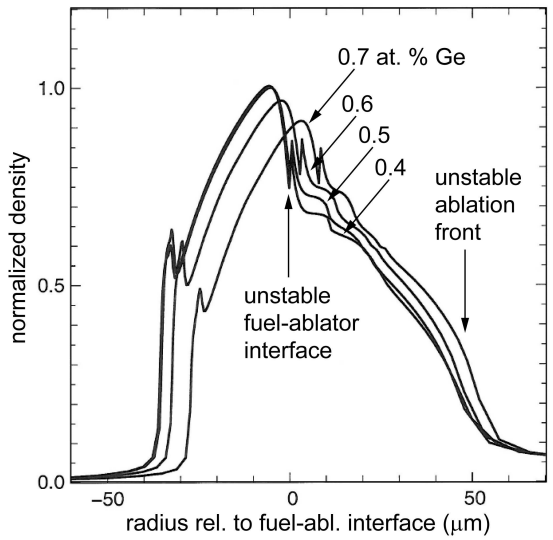

FIG. 5: Comparison of the different shell density profiles at peak implosion velocity resulting from different initial peak dopant concentrations. To avoid reducing the implosion velocity, the initial distributions are constrained so that the width of the dopant concentration scales as the inverse square root of the peak dopant concentration. At peak velocity, both the unstable Atwood number at the fuel-ablator interface and the ablation front scale length must be balanced for overall stability.

titatively, Fig. 6 plots fuel-ablator Atwood number (a) and ablation front scale length (b) for these four cases as functions of time close to the time of peak velocity. The trend of lower Atwood number at the cost of shorter ablation front scale lengths is evident. A rational balance between controlling the instability growth at the fuel-ablator interface without inducing excessive growth at the ablation front is to choose an intermediate dopant concentration with both a low Atwood number and moderate scale length. A germanium atom fraction of 0.5% was judged an appropriate balance. Note that 1-D considerations such as these are alone insufficient for determining the optimum balance of fuel-ablator Atwood number and ablation front scale length. Detailed 2-D simulations, such as those discussed below, are required to confirm that 0.5% is an appropriate value.

The design space of fuel thickness versus ablator thickness for an earlier version of this capsule was also scanned in the manner developed by Herrmann, *et al.* as described in Ref. [8]. That is, a suite of several hundred pairs of ablator and fuel thicknesses was run with the capsule outer radius fixed, roughly approximating constant capsule absorbed energy. The dopant concentration was held fixed, and the radiation pulse shape driving the capsule was re-tuned automatically for each pair. While scans such as these serve to give a broad survey of the parameter space and ensure that the particular design chosen (in the sense of ablator and fuel thickness) is not unduly close to a 1-D ignition cliff, detailed design assessments require extensive 2-D stability simulations. These simulations, described further below, are too computationally intensive to be run for each fuel ablator pair in the entire scan. Hence, while the design most centered in the 1-D ignition region in fuel thickness and ablator thickness can be treated as a starting point, considerations such as those in Fig. 6 suggest which design will be most optimal in balancing 1-D performance and 2-D stability, and those designs subsequently investigated in more detail. Generally, the capsule dimensions found most optimal with respect to both 2-D and 1-D considerations skew away from the center of the 1-D ignition region to regions of thicker ablators and thinner fuel layers.

IV. TWO-DIMENSIONAL LOW-MODE ROBUSTNESS

First among the 2-D simulations used to assess capsule robustness are low-mode simulations resolving the complete 180° angular extent of the capsule. This class of simulations resolve Legendre modes $\ell = 1 - 30$ with perturbations applied to all of the initial capsule interfaces: the inner ice surface, fuel-ablator interface, the internal dopant layers, and the outside of the ablator. These spectra are derived from measured surface data of fabricated capsule prototypes as well as simulation input of what roughnesses are tolerable [20]. Since the simulations are run in 2-D, the amplitude at each Legendre

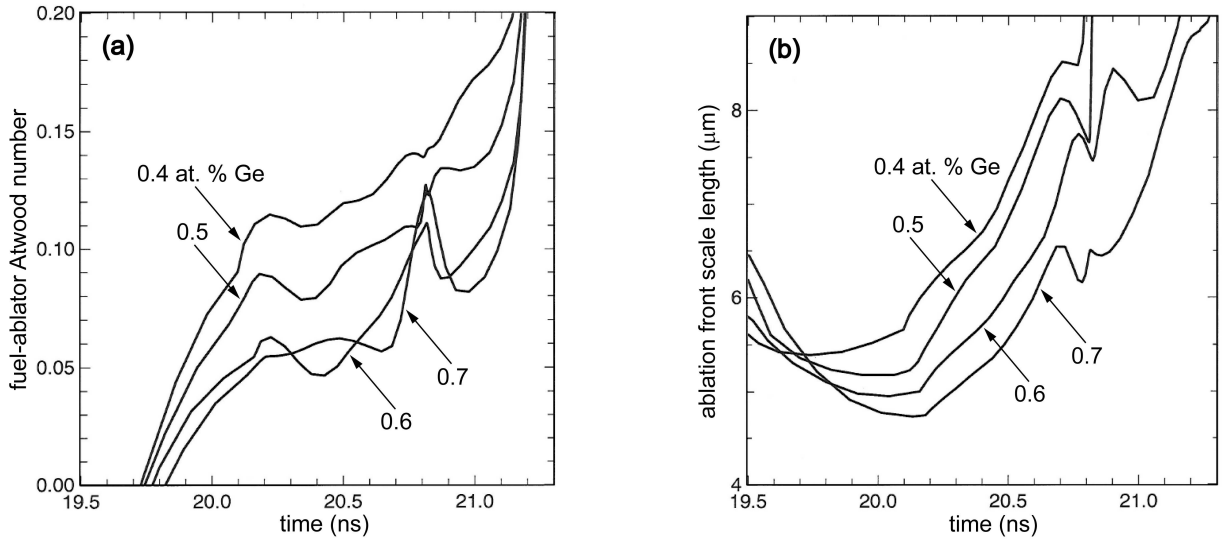

FIG. 6: Fuel-ablator Atwood number (a) and ablation front scale length (b) plotted as functions of time for the four dopant distributions of Fig. 5. The highest dopant concentration (0.7 at.%) gives the lowest Atwood number and most stable interface but also the shortest ablation front scale length and most unstable ablation front. To compromise between these two competing effects an optimum concentration of 0.5 at.% was chosen.

mode number is multiplied by $\sqrt{2\ell+1}$ to account for the $2\ell+1$ azimuthal m-modes which are present on a real 3-D capsule surface; it is assumed that each of these $2\ell+1$ modes adds incoherently. So long as all modes remain in the linear regime of RT growth, this prescription accurately captures the true 3-D nature of the growth. Since typical perturbations can grow into the weakly nonlinear regime, comparing these results against selected 3-D simulations is necessary [13]. Regrettably, fully 3-D simulations remain too computationally intensive to be run in the numbers necessary to scan fully the various capsule failure modes. Importantly, then, the 2-D simulations can be run sufficiently quickly to amass large data sets spanning the design space of interest.

An example of such a data set is presented in Fig. 7 which compares the robustness of the current CH capsule design to the 285 eV beryllium capsule design. The curves show normalized 2-D capsule yield versus multiplier on the roughness of the initial ice surface for modes $\ell = 1 - 30$. Since the initial ice roughness is a leading contributor to hot spot perturbations, applying a multiplier to the roughness is a good metric for overall capsule robustness. Apparently, the CH capsule can withstand an ice layer between three and four times the nominal roughness without a serious degradation in yield. By comparison, the beryllium yield curve shows a slightly lower tolerance of only two and a half to three times the nominal roughness. Note also that the yield curve for CH includes the expected roughness on all interfaces in addition to the ice, while the beryllium yield curve is for ice roughness only. Evidently, this CH design is more robust than the beryllium equivalent. This seemingly better performance of the CH capsule must be tempered, however, by noting that the less efficient CH ablator re-

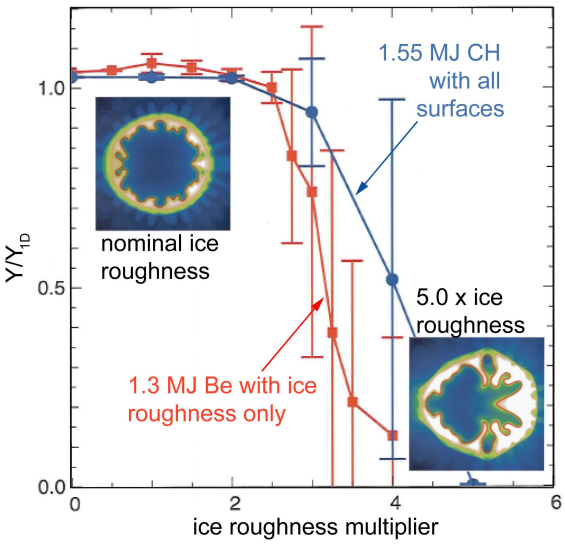

FIG. 7: (Color on-line) Capsule yield normalized to the 1-D value versus initial ice roughness for the 1.3 MJ beryllium ablator design (squares) and the 1.55 MJ CH design (circles). The 2-D simulations include roughness on all interfaces in Legendre modes $\ell = 1 - 30$, but only the roughness of the inner edge of the ice layer is multiplied. The higher energy CH design shows slightly greater robustness to low-mode perturbations than the beryllium counterpart. Each data point shown represents an average of seven simulations each with different realizations of the random surface roughnesses; the error bars give the variance of the yields. The insets show a nominal CH hot spot at the time of ignition only slightly perturbed from the 1-D and a failing hot spot resulting from an initial ice roughness five times the nominal value. The color scales give the relative density.

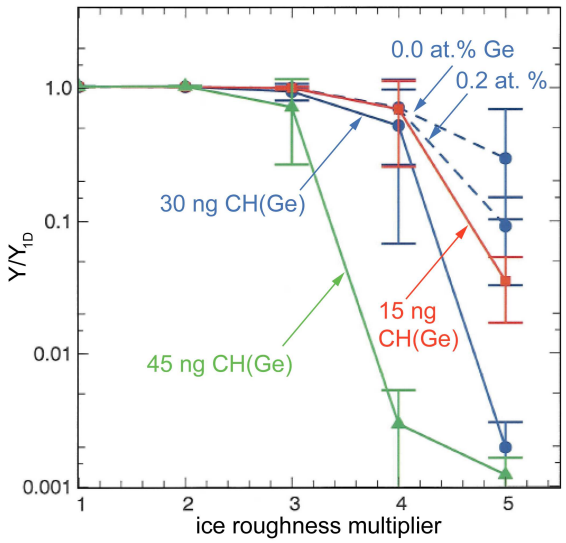

FIG. 8: (Color on-line) Effect of ablator mass injected by the fill tube perturbation on low-mode robustness. The nominal design (blue circles) assumes 30 ng of injected ablator material with 0.5 at.% germanium. A 50% increase to 45 ng (green triangles) reduces the tolerable ice roughness from approximately 4 to 3 times the nominal roughnesss. A decrease of the injected mass to 15 ng (red squares) only slightly increases the robustness. Shown by the dashed curves is the effect of varying the dopant concentration in the injected ablator mass for the nominal injected mass of 30 ng. The design assumes the most pessimistic value of 0.5 at.% germanium, *i.e.*, all of the mass originates from the most heavily doped layer. Reducing the dopant concentration in the injected mass to 0.2 and 0.0 at.% germanium only slightly increases robustness.

quired 1.55 MJ of laser drive to achieve this robustness, while the beryllium capsule was driven with only 1.3 MJ of energy. Nonetheless, roughness tolerances of approximately three times the nominal for this mode range are judged to represent acceptably robust capsule designs for either ablator.

For illustration, the two insets in Fig. 7 show example 2-D hot spots at the time of ignition, defined as the time when the central ion temperature first exceeds 12 keV. Both a robustly igniting CH capsule with nominal ice roughness and a failing capsule with five times the nominal roughness are shown. The large spikes penetrating the hot spot in the latter case cool and thereby reduce the effective hot spot volume to the point that ignition is never achieved. The color scales give the relative density.

Having established the baseline low-mode robustness of the capsule, these 180° simulations may also be used to evaluate the sensitivity of the design to deviations in other parameters. Fig. 8 shows the sensitivity of the yield curve to increasing or decreasing the mass of high-Z contamination present in the hot spot. As described above, the perturbation caused by the presence of the fill tube results in a jet of high-Z ablator material being injected into the hot spot. Extremely high resolution simulations [10, 12] suggest that 30 ng of mixed CH(Ge) material ultimately reaches the hot spot; in the simulations shown in Fig. 7, this mass of contaminant is included in the initial capsule gas fill. In Fig. 8, it is shown that halving the mass of contaminants to 15 ng does not significantly increase the robustness, while increasing the contaminant mass by 50% would be a noticeable loss in robustness. Given that there is some uncertainty in the amount of material that the fill tube will inject, that even a 50% increase does not have a catastrophic effect on the robustness reflects the overall viability of the design.

Also shown in Fig. 8 is the low-mode sensitivity to variations in the fraction of germanium in the injected contaminant. As a conservative assessment, the nominal case simulation of Fig. 7 assumed the injected mass was entirely from the most heavily doped layer, *i.e.*, composed of 0.5 at.% germanium. A germanium fraction closer to half of that is suggested by high-resolution simulations [12]. From Fig. 8, despite its very high-Z, reducing the germanium fraction in the contaminant proves only weakly to affect the robustness. Evidently, the much larger fractions of carbon and oxygen in the injected material is the dominating effect, rather than the small fraction of germanium.

Finally, as a validation of using these low-mode simulations to assess capsule robustness, they can be compared against higher resolution simulations including more Legendre modes but covering a smaller angular extent of the capsule. Fig. 9 compares a 180° simulation resolving $\ell = 1 - 30$ on the left to an analogous 90° simulation resolving $\ell = 2 - 60$ on the right. Since only half of the full capsule extent is simulated, the higher resolution simulation seeds perturbations only at the even numbered Legendre modes and the modal amplitudes are multiplied by $\sqrt{2}$ to account for the missing odd numbered modes. Fig. 9(a) compares both simulations at the time of peak implosion velocity when the ablation front growth has reached its maximum. The yellow line in each simulation denotes the unstable boundary between the DT fuel and the unburned ablator. Clearly, the presence of higher modes in the right simulation introduces considerably more perturbation to the shell. Extremely high mode simulations are required to resolve the growth at the fuel-ablator interface. Simulations by one of us (BAH), such as described in Ref. [12], have gone as high as mode 2,000 in 2-D and 3-D and also indicate growth similar to that described here.

Fig. 9(b) compares these same runs at ignition time. Focusing on the red line denoting the boundary of the igniting hot spot, both simulations suggest that the dominant perturbation to the hot spot occurs in the range of $\ell = 10 - 12$. At the time shown, the simulation on the left has a hot spot RMS perturbation of 2.83 μm, while the simulation on the right has the slightly higher RMS of 3.39 μm. By the end of the simulations, the lower resolution run has reached a yield of 18.5 MJ and the higher resolution case the slightly lower yield of 16.5 MJ. Nevertheless, that the higher resolution simulation reproduces the basic hot spot shape of the lower resolution simula-

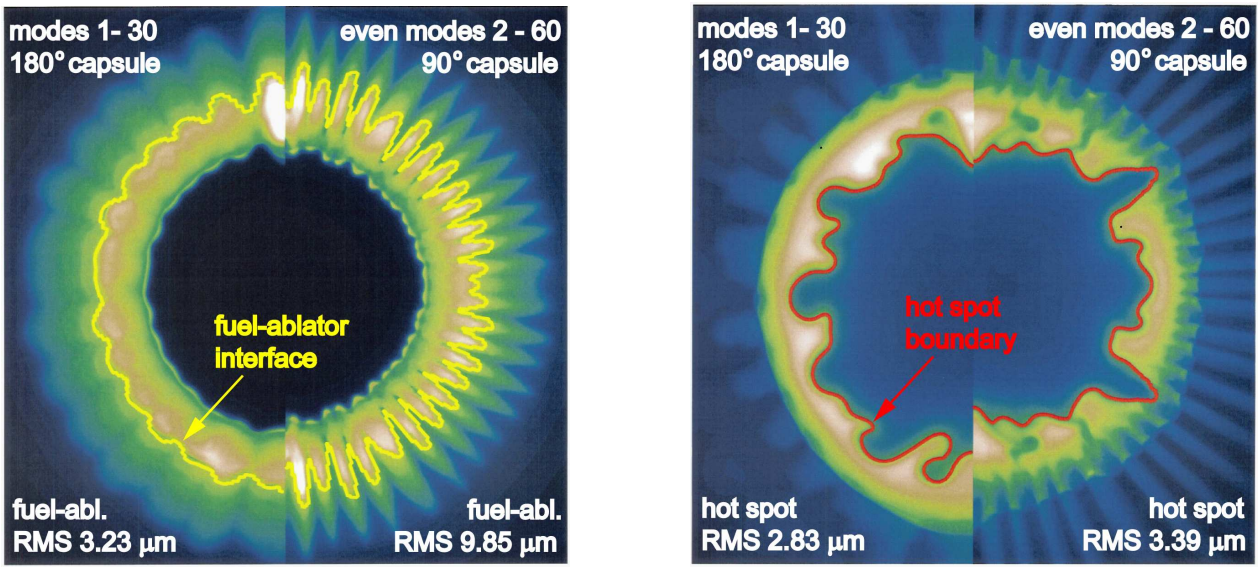

FIG. 9: (Color on-line) Comparisons of a 180° full-capsule simulation resolving Legendre modes $\ell = 1 - 30$ (left side) with more highly resolved 90° capsule simulation including even modes $\ell = 2 - 60$ (right side). The left panel compares the densities at peak implosion velocity, and the right panel the hot spots at ignition time. In the former, the yellow curve marks the fuel-ablator interface, and in the latter the red curve identifies the hot spot boundary. Nominal roughness spectra are included on all capsule interfaces. In the 90° case, the mode amplitudes are multiplied by $\sqrt{2}$ to account for the missing odd mode amplitude. Although the more highly resolved simulation shows peak velocity growth at higher modes than are included in the lower resolution simulation, the hot spot shapes at ignition time are roughly similar suggesting that the dominant effects are captured at the lower resolution.

tion validates simulating the robustness yield curve with resolution only up to mode $\ell = 30$. Some amount of feed-through of higher wavelengths is evident at higher resolution, particularly contributing to the large perturbation at 30° from the horizontal. A larger amount of mix on the outside of the dense fuel is also apparent in the higher resolution run. This high-mode mix can contribute to the reduced yield in the form of reduced averaged fuel compressibility and hence assembled areal density. Simulations with higher yet resolution are a subject of ongoing work.

V. INTERMEDIATE MODE STABILITY

While it is the low Legendre mode numbers which appear to dominate the perturbations of the hot spot, higher mode growth, especially at the ablation front, must also be considered in reaching an optimal capsule design. This is particularly true on account of two effects: the near-classical growth of perturbations at the fuel-ablator interface and the amplification of localized but relatively large perturbations to the capsule surface.

The first of these high-mode effects is suggested by the mix at the fuel-ablator interface evident in Fig. 9(b). As already described, the mixing of hot ablator material into the otherwise cold fuel caused by growth at this interface both reduces the yield and reduces margin by degrading the fuel compressibility. Absorption of x-ray preheat in the ablator results in a temperature differential between the fuel and ablator, producing a density gradient surrounding this interface that is unstable for much of the acceleration phase of the implosion. Indeed, it has been shown that mode numbers up to $\ell = 2,000$ contribute at this interface with stabilization introduced at higher modes due to the density gradient set by the conduction length [13]. Growth on the density gradient is seeded both by initial perturbations on the interface, and by coupling from growth at the ablation front. The coupling is more important for the CH ablator than for Be because of its lower initial mass. Properly resolving the growth at this interface requires very highly resolved simulations described elsewhere [12].

The fill tube perturbation is a prime example of the second of these higher mode effects, where a highly localized, large amplitude perturbation couples to short-wavelength unstable modes at the ablation front and can ultimately lead to a jetting of material into the hot spot. As already mentioned, a particular concern for CH ablators is the presence not only of the fill tube but also of defects or bumps on the shell surface. If these bumps are sufficiently large and present in sufficient numbers they could inject excessive ablator material into the hot spot and so quench ignition.

Since these defects have various shapes and sizes, understanding their growth in general is facilitated by simulations of single-mode linear-regime growth. These simulations are run with pure cosine perturbations of infinites-

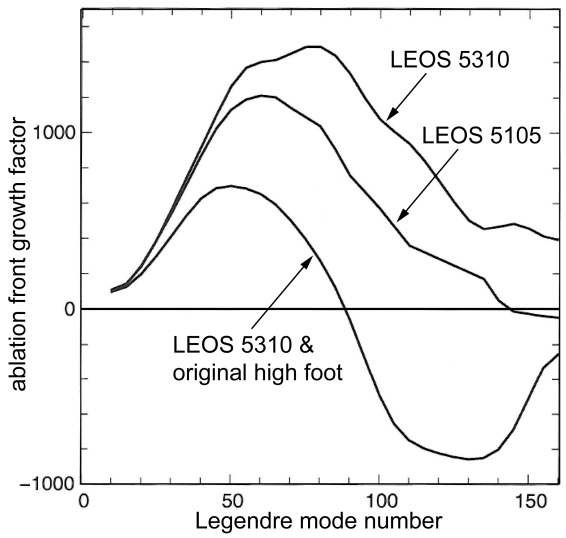

FIG. 10: Growth factors for ablator surface perturbations at peak velocity for Legendre mode numbers $\ell = 10 - 160$. Curves for the nominal CH equation of state, LEOS 5310, and an earlier, less compressible equation of state, LEOS 5105, are shown. The lower compressibility of the earlier EOS results in substantially less intermediate mode growth. Also shown are the lower growth factors that result from using an earlier high-foot pulse shape (shown in Fig. 2) with the nominal EOS. The stronger shock from the high foot pulse causes a change in sign of the ablation front growth for modes $\ell = 90 - 170$. These negative growth factors cause initially outward directed bumps of typical size to become inward directed bubbles penetrating into the accelerated shell.

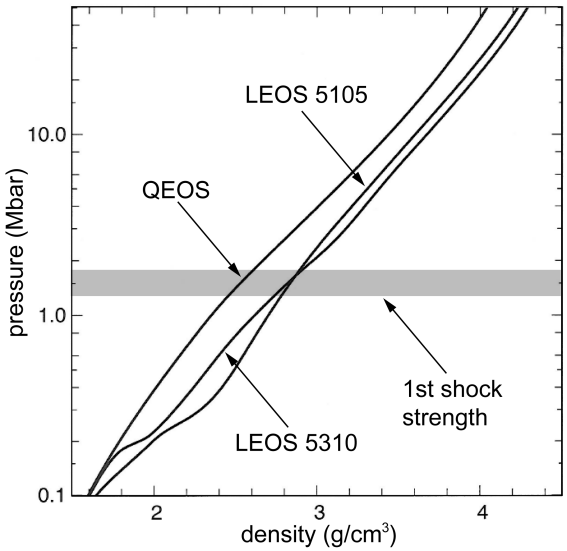

FIG. 11: Principle Hugoniots for three different EOS models used for CH: the analytic QEOS model and two tabular models LEOS 5105 and 5310. As shown in Fig. 10, a substantial increase in growth factors results from the increase in compressibility between LEOS 5105 and 5310. The shaded region highlights the pressures reached by the first shock as it transits the CH.

imal amplitudes applied to the outside of the ablator. A balance must be struck here between initializing a sufficiently small amplitude perturbation that it remains fully in the linear regime throughout the simulation and a sufficiently large amplitude that the perturbation is greater than the numerical noise threshold. Initial amplitudes of 10^{-7} cm have proven acceptable. The simulations are run purely Lagrangian, *i.e.*, without any grid relaxation. At the time of peak velocity, the ratios of the final ablation front perturbation to the initial ablator perturbation is extracted. Fig. 10 plots these growth factors for modes $\ell = 10 - 160$.

The peaking of the growth factor curves near $\ell = 100$ reflects both the onset of ablative stabilization and the phase oscillation of the growth during the early RM evolution. The amplitude oscillates during the shock transit phase at a mode-dependent rate, changing the effective initial amplitude at the onset of the RT phase. These oscillations have been analyzed theoretically and also observed in experiments [14].

A striking feature of the intermediate mode growth that can be gauged from these growth factors is the dependence on the CH equation of state. Early versions of the capsule design used the QEOS equation of state [15], and later a tabular equation of state, LEOS 5105. In the most recent revision of the design, a new tabular EOS, LEOS 5310, was used which was specifically tuned to match the most recent shock experiments on CH [16]. Fig. 11 compares the principle Hugoniots of these three EOSs. The shaded region marks the pressures accessed by the first shock as it transits the ablator with a strength of $1.3 - 2.3$ Mbar. The trend toward higher compressibility with the newer tables is evident. The corresponding impact on the ablation front growth factors of the two different EOS tables is shown in Fig. 10. The higher compressibility of the newer EOS, as validated in experiments, leads to significantly more early-time, RM growth which, after amplification by RT growth, leads to significantly higher growth factors at peak velocity. As noted in Sec. II, this enhancement of the growth with increased compressibility has progressively driven the design to using thicker ablators at the cost of lower implosion velocity. Of course, it must be recognized that the EOS of CH cannot be known with perfect precision. The variability illustrated by Figs. 10 hence underscores the importance of a design with robust performance margins to uncertainties in the amount of RM and RT growth.

The intermediate mode growth factors have also been found to be sensitive to the strength of the first shock crossing the ablator. An earlier version of the capsule design used a higher picket in the foot of the radiation drive to launch a $1.6 - 4.0$ Mbar first shock, compared to the $1.3 - 2.3$ Mbar shock of the current design. This earlier pulse shape is shown as the dashed curve in Fig. 2. The dramatic swing in the ablation front growth factors that results from this different drive is also shown in Fig. 10. Physically, this is again an effect of the phasing of the RM

oscillations with respect to the onset of the RT growth phase.

Initially, it might appear that the growth factors with the stronger first shock are on average lower than with the lower foot and would therefore lead to less growth and a less perturbed implosion at peak velocity. Multimode simulations seeding all modes $\ell = 1 - 160$ on a 15° sector indeed bear this out. However, the negative growth factors for modes in the range of $\ell = 100 - 150$ have an important effect with respect to the isolated surface bumps characteristic of the CH ablator surface.

The sensitivity to shock strength, EOS, and perturbation sign were first noted by one of us (BAH) in highly resolved simulations with the massively parallel HYDRA code [17]. These results are described elsewhere [12]. Complementary simulations were also run using LASNEX on 5° polar wedges with Gaussian perturbations on the ablator surface with 10 μm half widths and variable heights. Fig. 12 compares the results with the different pulse shapes from LASNEX simulations. Though the ablation front growth factors seem in an average sense lower with the higher foot, the fact that the growth factors are negative with the higher foot causes the initially outward pointing bumps, localized near $\ell = 100-150$, to grow into inward pointing bubbles. When the initial bump amplitude exceeds ~ 300 nm, the bump totally penetrates the shell and could be expected to inject further ablator material into the hot spot in addition to the fill tube contribution. By contrast, the positive and slightly lower growth factors in the $100 - 150$ mode number range with the lower foot cause similar bumps merely to grow into localized perturbations at the fuel-ablator interface and do not appear to compromise the shell. An outgoing spike that would be predicted by linear analysis based on the growth factors is burnt off. These simulations and the HYDRA simulations as described elsewhere indicate that surface bumps typical of those seen on CH shells can lead to bubbles that penetrate the shell and inject a few nanograms of material into the hot spot. The amount of penetration depends on the CH equation of state, the foot level, and the sign of the initial defect.

In addition to outward bumps, target characterization indicates that CH shells also display a slightly smaller number of inward-directed divots. Of course, the positive growth factors with the low foot will cause these to amplify into inward-going bubbles which could threaten the shell's integrity. That the growth factors in the $\ell = 100-150$ range are somewhat lower in absolute value for the low foot than for the high foot indicates that the penetration of these inward bumps will be not as severe as the analogous outward bump in the high foot case. Since we cannot expect to model these effects with perfect accuracy, it is important that the plans for ignition include some margin with respect to the bumps on the CH ablator.

VI. STATISTICAL ASSESSMENTS OF ROBUSTNESS

In addition to optimizing the capsule design in 1-D and ensuring its stability in 2-D, it is important to recognize that a variety of random defects can occur in any given capsule or in the laser performance from shot to shot. Hence, capsule robustness is important not only with respect to 2-D imperfections but also to random variations in, for example, the capsule radial dimensions, material compositions, and radiation pulse shape. Assessing this aspect of robustness requires a statistical approach.

The approach followed here was developed by Salmonson for the beryllium ablator design [18]. It consists of tabulating as many as possible random sources of error to be expected under actual experimental conditions, bracketing those sources of error within specified bounds and with specified statistical distributions, and then generating a data set of random instantiations of the given capsule design with these sources of error. Generally, Gaussian distributions are used for physics uncertainties such as pulse shape levels and times, and uniform distributions are chosen for capsule dimensions, dopant concentrations, etc. Since the latter are subject to measurement, it is assumed that targets are fabricated with somewhat greater variations, and then outliers are rejected. The list of individual deviations is too extensive to enumerate here but includes all aspects of the capsule dimensions, dopant concentrations, material compositions and densities, pulse shaping parameters, and expected contaminants.

Once the full data set of capsules has been run, the simulations may be post-processed to extract, for example, the distribution of expected yields given the assumed uncertainty or the capsule ignition threshold. Typically, the data set is generated in two steps by first running a large number of 1-D simulations including all 1-D sources of error, and then sub-sampling this data set to rerun randomly selected instantiations in 2-D with random surface perturbations. In this way, a fairly realistic picture of the expected capsule performance, its mean and distribution, can be generated.

Fig. 13 summarizes the results of such a study on the current CH capsule design. Fig. 13(a) plots the distribution of yields to be expected from three iterations of this study: The red curve gives the yield distribution including all 1-D errors with all deviations set to their nominal values, *i.e.*, as expected under experimental conditions. There are 10,000 total instantiations sampled. The blue curve gives a similar distribution of 1-D yields but with deviations drawn from distributions with twice the width of the nominal distributions. This doubling applies to all error sources except for the capsule outer radius, ablator and fuel thicknesses, and the peak flux of the radiation drive. These four parameters are excluded since they have very strong influences on the yield and, if doubled, lead to meaninglessly broad distributions in yield. This doubling of the deviations is useful in assessing the over-

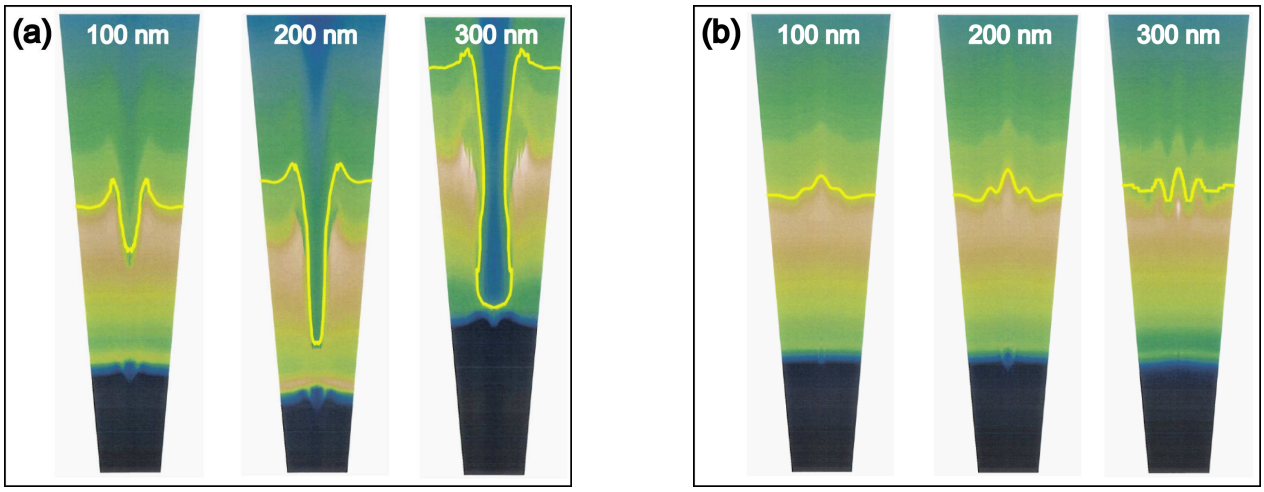

FIG. 12: (Color on-line) Results of isolated bump simulations using the original high foot pulse shape (a) and the revised low foot pulse shape (b). Both sets of simulations used 10 μm full width Gaussian bumps on the ablator surface with initial heights of 100, 200, and 300 nm. The yellow curves identify the fuel-ablator interface at peak velocity. For a 300 nm bump, the shell is completely penetrated with the high foot pulse shape but is only weakly perturbed in the low foot case.

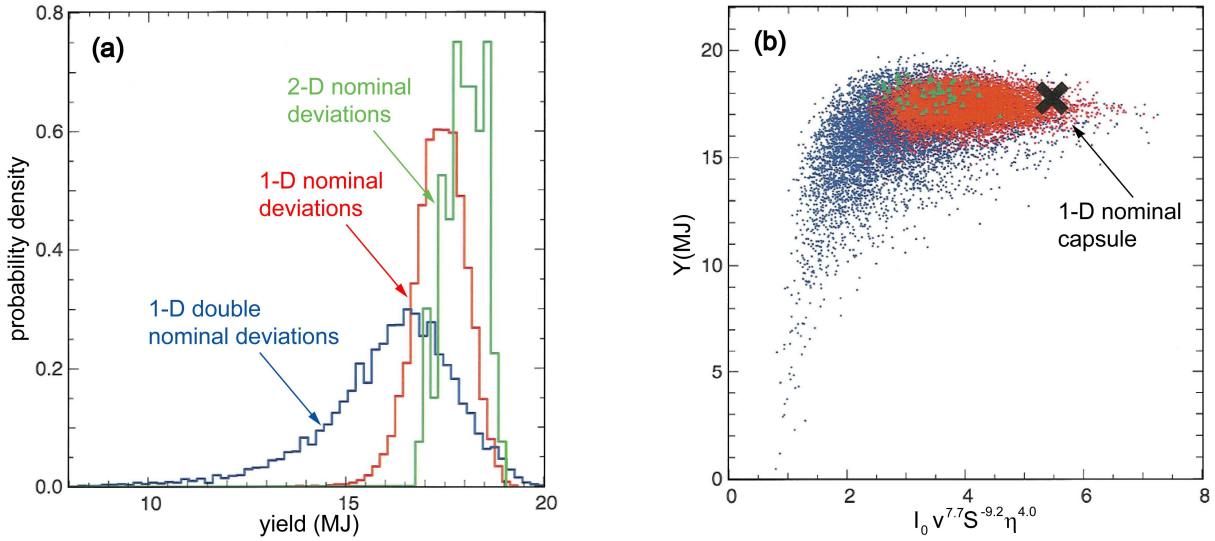

FIG. 13: (Color on-line) Results of statistical scans over all expected capsule defects summarized as yield distribution functions (a) and a scatter plot of yield versus Ignition Threshold Factor (ITF) (b). The red ensemble is the result of 10,000 1-D samples with nominal deviations, the blue ensemble is the result of 10,000 1-D samples with double nominal deviations, and the green ensemble results from sub-sampling the 1-D nominal ensemble into 2-D including random roughnesses on all interfaces for a total of seventy realizations. The distributions of yield indicate that none of the capsules failed in 1-D or 2-D with nominal deviations, while the scatter plot of capsule ITF shows that an ITF of 5.5 can be expected for the design in 1-D and approximately 3.0 in 2-D.

all sensitivity of yield to each of the deviations and also in the context of the ignition threshold discussed below.

Finally, the green curve gives the result of sub-sampling the original 1-D nominal distribution into 2-D. The green data set consists of randomly selecting ten instantiations from the 10,000 1-D samples with nominal deviations. Each of these is then run in 2-D with low mode perturbations on all interfaces and using seven different realizations of the surface roughnesses for a total 2-D data set of seventy runs. These simulations are analogous to the low-mode simulations described in Sec. IV.

What is immediately evident from Fig. 13(a) is that the CH capsule design is highly robust in 1-D as well as 2-D. With nominal deviations, none of the capsules sampled in 1-D or 2-D failed in the sense of yielding less than 1.0 MJ. Indeed, the lowest yield in this combined data set was 13.8 MJ. Even with the deviations doubled in 1-D, only one instantiation gave a yield less than 1.0 MJ.

While these results are encouraging that ignition can be robustly achieved with this capsule design, especially those simulations in 2-D, two important caveats should be borne in mind. These are that the 2-D simulations do not include two known important deviations that degrade yield: low-mode asymmetries present in the radiation drive and high-mode mix at the fuel ablator interface. It is precisely to provide margin to these remaining uncertainties that the capsule was designed to be so robust in 1-D and with respect to 2-D low-mode perturbations. The inclusion of these two remaining sources of error in similar scans is a subject of continuing work.

Another way of analyzing the data set is to plot capsule yield versus Ignition Threshold Factor (ITF), as shown in Fig. 13(b). The abscissa in this plot is the ITF, a measure of capsule performance relative to the threshold of ignition and previously referred to as capsule margin [21]. As given in the figure, ITF can be represented as a product of implosion velocity v, fuel averaged entropy S, and hot spot perturbation fraction η and has been shown to be a reliable predictor of capsule performance [19]. The overall normalization constant I_0 is set so that the ignition cliff is located at an ITF of 1.0. Here the different colored clouds of dots correspond to the same three distributions of runs as in Fig. 13(a): each red dot represents one instantiation of the 1-D nominal deviations, each blue dot an instantiation of the 1-D double nominal deviations, and each green triangle a 2-D realization of the nominal deviations.

In Fig. 13(b), the utility of generating a data set with double nominal deviations becomes apparent. This is because it is only by identifying the location of the yield cliff that the capsule ITF can be normalized. By definition, this cliff occurs at an ITF of 1.0; relying only on the data set of nominal deviations, the location of the cliff is ambiguous. With this normalization, the nominal 1-D design, *i.e.*, without any deviations, can be located at an ITF of 5.5, as denoted by the black "X." With the addition of 1-D nominal deviations, the ITF is degraded to between 2.0 and 5.0. In a few instances, the ITF apparently increases due to the deviations; this corresponds to an increase in velocity, resulting for example from lower than nominal oxygen in the ablator. An analysis including high-mode instability growth, which is beyond the scope of this paper, shows that the overall ITF is generally reduced for such points. With the addition of 1-D double nominal deviations, the distribution of ITF increases further, and the location of the yield cliff becomes evident. Finally, the cloud of green triangles indicates that with nominal deviations and nominal 2-D low-mode perturbations an average ITF of approximately 3.0 can be expected. Again, this is without including radiation drive asymmetries and high-mode fuel-ablator mix. These effects will further reduce the available ITF but are judged not to degrade it beyond the ignition cliff at ITF = 1.0.

VII. CONTINUING DESIGN EVOLUTION

As noted in Sec. I, at best a given capsule design is a snapshot of a continually evolving optimum. As improved physics models are included in simulations and, more importantly, as experimental data becomes available to anchor simulation results, capsule designs are continually refined to reflect the most accurate available physics understanding. Recently, a similar modification has been made to the CH capsule design described in the preceding sections. In light of continuing concern over the presence of localized defects on the ablator surface and the possibility that each of these "bumps," if sufficiently large could inject ~ 5 ng of material into the hot spot, the design has been further modified to improve intermediate- and high-mode stability at the expense of low-mode stability. As shown in Sec. V, the growth at intermediate modes is sensitive to both the CH equation of state and to the level of the first shock. Despite optimizing the design with the best available models of the EOS and expected radiation drive, residual uncertainties in these important factors, of course, remain. Hence, although the results of Sec. V suggest that the known isolated defects should not grow unacceptably, it is prudent to further increase the designs margin to high-mode growth relative to the uncertainty in this growth.

To increase the capsule robustness to intermediate-mode growth the ablator thickness was slightly increased from 190 to 200 μm and the fuel thickness was slightly reduced from 65 to 63 μm while maintaining the capsule outer radius unchanged. This change represents the distinction between Rev. 4 draft 1 and Rev. 4 final as depicted in Fig. 1. By reducing the fuel thickness, some of the implosion velocity lost by thickening the ablator can be regained, and only a small net reduction in implosion velocity, from 0.384 mm/ns to 0.379 mm/ns, is incurred.

The effect of these design changes on stability and robustness is summarized in Fig. 14. Fig. 14(a) shows the $\sim$ 15% reduction in peak ablation front growth factor that can be acheived in this way, while Fig. 14(b) shows the effective cost of this growth factor reduction. That is, the tolerable ice surface roughness is reduced from nearly four times the nominal roughness to approximately three times. Without increasing the capsule scale or energy, this example illustrates well the obligatory trade-offs that must be made between intermediate- and high-mode stability on the one hand and low-mode robustness on the other.

Even more recently, the first experimental data from NIF has begun to suggest that the hard x-ray content (gold M-band flux) of the radiation spectrum within NIF hohlraums is larger than anticipated. In response, the CH capsule design is currently being further redesigned. To accommodate the higher M-band, the germanium dopant concentration is being increased. Such modifications can be expected to continue as further experimental data become available on capsule and hohlraum performance and ultimately until the capsule design is proven

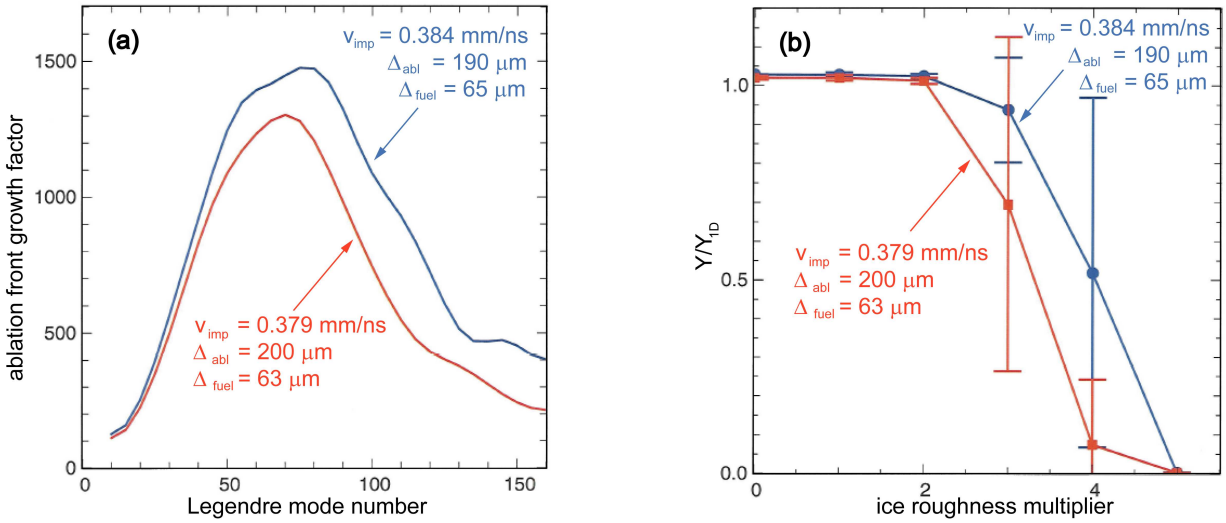

FIG. 14: (Color on-line) Ablation front growth factors and low-mode yield curves for the final modification of the Rev. 4 design (red) as compared to the draft 1 design (blue). By increasing the ablator thickness and thereby reducing the implosion velocity, the ablation front growth factors were reduced but at the cost of reduced low-mode robustness.

adequate to achieve ignition.

VIII. CONCLUSIONS

This paper has summarized the current state of the plastic ablator ignition capsule design for NIF. Broadly, a balance has been sought between the many competing considerations of 1-D performance optimization, 2-D stability requirements, and 1-D and 2-D statistical reliability in an effort to reach a design most likely to achieve ignition. First, a 1-D design was developed which both gave good performance in the sense of low fuel entropy and high implosion velocity for the allowed laser energy, and also struck a balance between a low fuel-ablator Atwood number and a moderate ablation front scale length, both important parameters in determining the growth of hydrodynamic instabilities in 2-D. The low-mode robustness of the design was assessed in full-capsule simulations including perturbations up to Legendre mode $\ell = 30$. Single-mode growth factor simulations were also used to assess the growth for mode numbers $\ell = 1-160$. The considerable sensitivity of these growth factors to both the equation of state used to model CH and to the strength of the first shock impinging on the capsule were highlighted by these simulations. On account of the expected presence of some number of isolated defects on the surface of CH capsules and their strong amplification in the neighborhood of $\ell \simeq 150$, the capsule design was slightly modified to emphasize intermediate and high-mode stability at the expense of low-mode robustness. Finally, statistical assessments of the likelihood of ignition including all anticipated 1-D sources of error as well as 2-D surface roughness suggest a high probability of ignition. The assessment described here did not include high-mode fuel-ablator mix or radiation drive asymmetries; estimates that will be described elsewhere indicate that the probability of ignition remains close to unity when these are included. Further revisions of the design necessarily continue as physics understanding improves and new experimental data become available.

Acknowledgments

This work was performed under the auspices of the U. S. Department of Energy by Lawrence Livermore National Laboratory under Contract DE-AC52-07NA27344.

[1] G. H. Miller, E. I. Moses, and C. R. Wuest, Nucl. Fusion **44**, S228 (2004).
[2] E. I. Moses, R. N. Boyd, B. A. Remington, C. J. Keane, and R. Al-Ayat, Phys. Plasmas **16**, 041006 (2009).
[3] J. D. Lindl, P. Amendt, R. L. Berger, et al., Phys. Plasmas **11**, 339 (2004).
[4] J. D. Lindl, *Inertial Confinement Fusion: the Quest for Ignition and Energy Gain Using Indirect Drive* (American Institute of Physics, New York, 1998).
[5] W. J. Krauser, N. M. Hoffman, D. C. Wilson, B. H. Wilde, W. S. Varnum, D. B. Harris, F. J. Swenson, P. A. Bradley, S. W. Haan, S. M. Pollaine, et al., Phys. Plasmas **3**, 2084 (1996).
[6] D. C. Wilson, P. A. Bradley, N. M. Hoffman, F. J. Swenson, D. P. Smitherman, R. E. Chrien, R. W. Margevicius, D. J. Thoma, L. R. Foreman, J. K. Hoffer, et al.,

Phys. Plasmas **5**, 1953 (1998).
[7] T. R. Dittrich, S. W. Haan, M. M. Marinak, S. Pollaine, and R. McEachern, Phys. Plasmas **5**, 3708 (1998).
[8] S. W. Haan, M. C. Herrmann, T. R. Dittrich, A. J. Fetterman, M. M. Marinak, D. H. Munro, S. M. Pollaine, J. D. Salmonson, G. L. Strobel, and L. J. Suter, Phys. Plasmas **12**, 056316 (2005).
[9] G. B. Zimmerman and W. L. Kruer, Comments Plasma Phys. and Controlled Fusion **2**, 51 (1975).
[10] J. Edwards, M. Marinak, T. Dittrich, S. Haan, J. Sanchez, J. Klingmann, and J. Moody, Phys. Plasmas **5**, 056318 (2005).
[11] J. D. Salmonson, Private Communication (2007).
[12] B. A. Hammel, S. W. Haan, D. Clark, M. J. Edwards, S. H. Langer, M. Marinak, M. Patel, J. Salmonson, and H. A. Scott, in *2nd International Conference on High Energy Density Physics* (Elsevier, Austin, TX, 2009).
[13] B. A. Hammel, M. J. Edwards, S. W. Haan, M. M. Marinak, M. Patel, H. Robey, and J. Salmonson, J. Phys.: Conf. Series **112**, 022007 (2008).
[14] Y. Aglitskiy, A. L. Velikovich, M. Karasik, V. Serlin, C. J. Pawley, A. J. Schmitt, S. P. Obenschain, A. N. Mostovych, J. H. Gardner, , et al., Phys. Plasmas **9**, 2264 (2002).
[15] R. M. More, K. H. Warren, D. A. Young, and G. B. Zimmerman, Phys. Fluids **31**, 3059 (1988).
[16] M. A. Barrios, D. G. Hicks, T. R. Boehly, D. E. Fratanduono, J. H. Eggert, P. M. Cellier, G. W. Collins, and D. D. Meyerhofer, *High-precision measurements of the equation of state (EOS) of polymers at 1 to 100 Mbar using laser-driven shock waves*, submitted to Phys. Plasmas (2009).
[17] M. M. Marinak, G. D. Kerbel, N. A. Gentile, O. Jones, D. Munro, S. Pollaine, T. R. Dittrich, and S. W. Haan, Phys. Plasmas **8**, 2275 (2001).
[18] J. D. Salmonson, Bull. Am. Phys. Soc. **52**, 273 (2007).
[19] D. S. Clark, S. W. Haan, and J. D. Salmonson, Phys. Plasmas **15**, 056305 (2008).
[20] The roughness power spectra are given by the following formulae. The spherical harmonic coefficients for the DT ice surface and the inside of the ablator shell are given by

$$R_{\ell m}^{\rm ice} = \frac{1.74}{\ell^{1.1}}$$

$$R_{\ell m}^{\rm inside} = \frac{300.0}{\ell^{2.3}} + \frac{0.06}{(\ell/70.0)^{0.6} + (\ell/1200.0)^{3.5}} \, .$$

The roughness of the outer ablator shell is given by a thickness perturbation which adds to $R_{\ell m}^{\rm inside}$ with a random sign:

$$\Delta R_{\ell m}^{\rm outside} = \frac{90.0}{\ell^{2.3}} + \frac{0.20}{(\ell/70.0)^{0.6} + (\ell/1200.0)^{3.5}} \, .$$

For modes $\ell \leq 12$, corrections are made individually to the amplitudes to agree with measured surfaces. These 3-D surface coefficients are converted to 2-D coefficients by multiplying each by the square root of the number of m-modes that would contribute in 3-D

$$R_{\ell}^{\rm 2D} = \pm\sqrt{2\ell+1} R_{\ell m}$$

where the sign of the coefficient is chosen randomly for each mode. For the four internal dopant layers, the spectral coefficients are assumed to be one fifth the power of the outer ablator surface and the surface perturbations to add successively until the last dopant surface is defined. Note that this prescription applies for modes $\ell = 1 - 30$. For higher modes, a more complicated prescription is required which progressively decorrelates the outer surface from inner surfaces with increasing mode number.
[21] The intuitive sense of margin M is better captured by defining it as $M = \mathrm{ITF} - 1$. By this definition, margin measures the distance from the ignition cliff in units of ITF. At the ignition cliff, where ITF $\equiv 1$, $M = 0$ and there is then no "margin."